*Structural Durability & Health Monitoring*

Tech Science Press

# Strain Transfer Mechanism of Grating Ends Fiber Bragg Grating for Structural Health Monitoring

**Guang Chen[1,*], Keqin Ding[1], Qibo Feng[2], Xinran Yin[1] and Fangxiong Tang[1]**

[1]China Special Equipment Inspection and Research Institute, Beijing, 10013, China.

[2]School of Science, Beijing Jiaotong University, Beijing, 100044, China.

[*]Corresponding Author: Guang Chen. Email: chenguagn015@163.com.

**Abstract:** The grating ends bonding fiber Bragg grating (FBG) sensor has been widely used in sensor packages such as substrate type and clamp type for health monitoring of large structures. However, owing to the shear deformation of the adhesive layer of FBG, the strain measured by FBG is often different from the strain of actual matrix, which causes strain measurement errors. This investigation aims at improving the measurement accuracy of strain for the grating ends surface-bonded FBG. To fulfill this objective, a strain transfer equation of the grating ends bonding FBG is derived, and a theoretical model of the average strain transfer from the matrix to the optical fiber is developed. Moreover, parameters that influence the average strain transfer rate from the matrix to the optical fiber are analyzed. A selection scheme of bonding parameters by numerical simulation is provided, which is significantly advantageous over that of the grating bonding FBG. The theoretical equation is verified by finite element method (FEM). Compared with the existing model, the proposed model has higher measurement accuracy. Experimental tests are performed to validate the effectiveness of the proposed model on the equal-intensity cantilever beam, whose surface is attached to the bare FBG with grating ends bonding and strain gauge by using epoxy glue. The results show that there is a great agreement between the outcome of the bare FBG and that of the strain gauge, and the corrected strain is closer to the true strain. The proposed model provides a theoretical basis for the design of the grating ends surface-bonded FBG strain sensor for health monitoring of large structures.

**Keywords:** Structural health monitoring; grating ends bonding; fiber Bragg grating; the average strain transfer; shear-lag theory

## 1 Introduction

It is one of the research hotspots in the field of structural health monitoring that FBG sensors are used for performance monitoring of large structures by virtue of their advantages of light weight, small dimensions, immunity to electromagnetic interference ability, and high sensitivity. When FBG is applied to the stress monitoring of the matrix, there is the strain transfer loss due to the existence of the adhesive layer, which makes the strain measured by FBG is different from the strain of matrix [1]. In order to improve the measurement accuracy of strain for the grating ends surface-bonded FBG, the influence of the adhesive layer should be taken into consideration to modify the strain value measured by FBG. Therefore, most researches concentrated on the relationship between the measured strain of FBG and the strain of the matrix under the influence of the adhesive layer and made a large number of achievements. For example, Many researchers [2-13] adopted certain assumed conditions to obtain the transfer characteristics of embedded FBG strain sensors. Other researchers [14-20] deduced the strain transfer equation of the surface bonded FBG sensors. However, the above studies mainly focus on the strain transfer of grating bonded packaged FBG sensors. The grating bonded packaged sensors is easy to occur

multi-peak phenomenon due to the force uncertainty of small-scale adhesive layer in the grating area, which result in wrong judgment of signal demodulation. The grating ends packaged sensors only bear force at both ends of FBG instead of the grating, which enable all points of the grating under the same stress and effectively avoid multi-peak problems of grating bonded packaged sensors. According to the principle of equivalent deformation, "Wu et al. [21] deduced the strain transfer function of the grating ends packaged structure", in which only the Young's modulus of the adhesive layer and the grating length were taken into account. "Sun et al. [22] proposed the strain transfer model for a clamped FBG sensor" based on symmetry.

In this paper, the theoretical model is proposed to predict the average strain transfer rate from the matrix through the adhesive layer to the optical fiber, which is different from existing surface-bonded models. A numerical study is performed to evaluate the sensor parameters that affect the average strain transfer rate. The validity of the theoretical equation is verified by finite element method and experiment.

## 2 Strain Transfer Mechanism of the Grating Ends Surface-Bonded FBG

The grating ends surface-bonded FBG consists of the matrix, optical fiber (removing the coating) and the adhesive layer, as shown in Fig. 1, optical fiber of removing the coating layer on both ends of FBG is attached on the matrix through the adhesive layer after pre-stressing is applied.

When the matrix is subjected to an external axial force, the deformation of the optical fiber both ends of FBG induced by the matrix is transferred through the adhesive layer, which induces a change of FBG reflection wavelength. In Fig. 1, FBG serves as a sensing element, whose grating is not directly contact with the adhesive layer. Fig. 2 shows the cross section of the grating ends surface-bonded FBG. Fig. 3 is the stress distribution of the grating ends surface-bonded FBG according to Fig. 1.

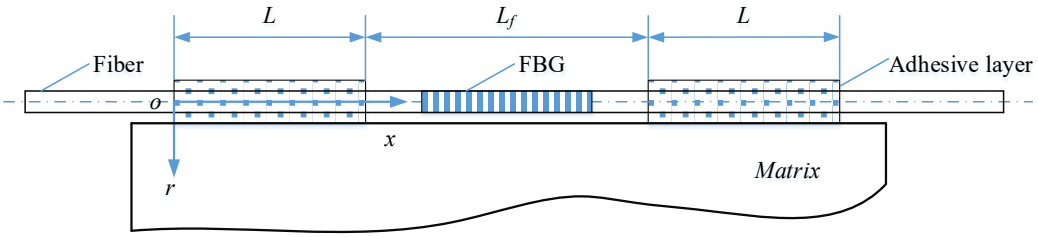


**Figure 1:** Model of the grating ends surface-bonded FBG

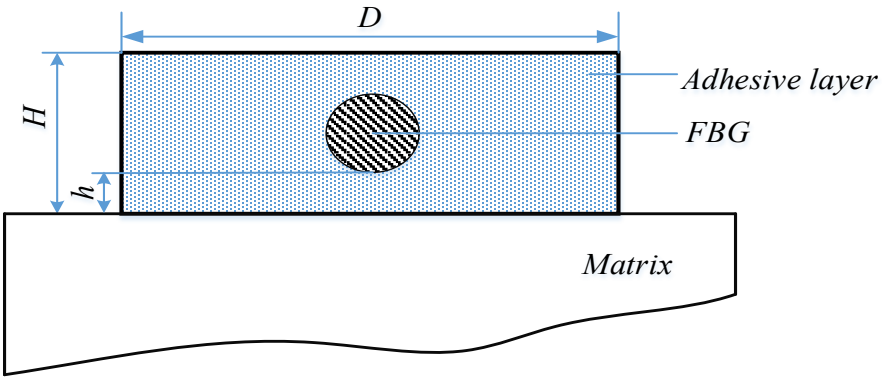


**Figure 2:** Cross section of the grating ends surface-bonded FBG

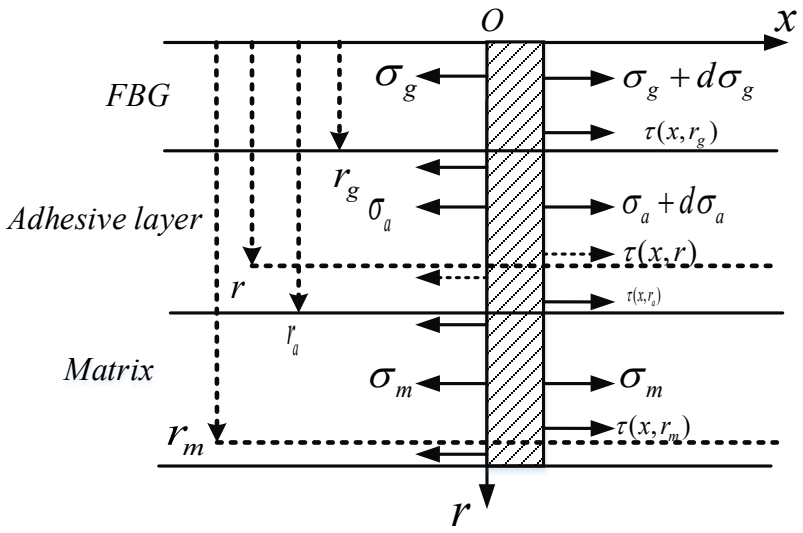


**Figure 3:** Stress distribution of the grating ends surface-bonded FBG

Strain transfer characteristics between the matrix and surface-bonded FBG are derived based on the following assumptions [5,14,17]: (1) Mechanical behavior of the bare fiber, adhesive layer and matrix are linear elastic isotropic materials. (2) Only the matrix is subjected to uniform axial stress, whereas the fiber and adhesive layer do not carry external loadings directly. (3) All the interfaces are perfectly bonded so that the displacements are consistent along the interfaces. (4) The temperature effects are not considered. (5) There is shear stress within a certain range of the matrix because of adhesive layer.

In this paper, σ, τ, ε and γ are the axial stress, shear stress, axial strain and shear strain, respectively. E, G, and μ are Young's modulus, shear modulus, and Poisson's ratio, respectively. u and v are the axial displacement and radial displacement, respectively. L, D, H and h represent the single bonding length the bonding width, the bonding height and the bottom thickness of the adhesive layer at one end, respectively. $L_f$ is the gauge length. The subscripts g, a and m represent the parameters associated to the optical fiber, the adhesive layer and the matrix, respectively. *r* denotes the spatial variable along the radial of the optical fiber.

The equilibrium equation for infinitesimal section *dx* of optical fiber in Fig. 3 is as follows.

$$\pi r_g^2 \sigma_g = \pi r_g^2 (\sigma_g + d\sigma_g) + 2\pi r_g \tau(x, r_g) dx \tag{1}$$

$$\tau(x, r_g) = -\frac{r_g}{2} \frac{d\sigma_g}{dx} \tag{2}$$

The following equation is used for the analysis of infinitesimal adhesive layer.

$$\left[ D(H - r_g - h + r) - \pi r_g^2 \right] \sigma_a + 2\pi r_g \tau(x, r_g) dx = \left[ D(H - r_g - h + r) - \pi r_g^2 \right] (d\sigma_a + \sigma_a) + \tau(x, r) D dx \tag{3}$$

$(r_g < r < r_a)$

Substitute Eq. (2) into Eq. (3):

$$\tau(x, r) = -\frac{\left[ D\left(H - r_g - h + r\right) - \pi r_g^2 \right]}{D} \frac{d\sigma_a}{dx} - \frac{\pi r_g^2}{D} \frac{d\sigma_g}{dx} \tag{4}$$

$\left(r_g < r < r_a\right)$

Similarly, the analysis of infinitesimal matrix affected by adhesive layer is shown as Eq. (4).

$$D(r-r_a)\sigma_m + Ddx\tau(x,r_a) = D(r-r_a)(\sigma_m + d\sigma_m) + Ddx\tau(x,r) \quad (r_a < r < r_m) \tag{5}$$

$$\tau(x,r) = \tau(x,r_a) - (r-r_a)\frac{d\sigma_m}{dx} \quad (r_a < r < r_m) \tag{6}$$

When r > $r_m$, there is no shear stress outside of the matrix. The boundary conditions are as follows.

$$\tau(x,r_m) = 0 \tag{7}$$

By Eq. (6) and Eq. (7), yields

$$\tau(x,r) = \left(\frac{r_m - r}{r_m - r_a}\right)\tau(x,r_a) \qquad (r_a < r < r_m) \tag{8}$$

According to the stress-strain relationship:

$$\begin{cases} \sigma = E\varepsilon \\ \tau = G\gamma \end{cases} \tag{9}$$

Supposing that the optical fiber deforms synchronously with as the adhesive layer is approximately the same, Eq. (10) can be obtained.

$$\frac{d\varepsilon_g}{dx} \cong \frac{d\varepsilon_a}{dx} \tag{10}$$

By Eq. (4), Eq. (8) and Eq. (10), yields

$$\tau(x,r) = -\frac{\left[D(H - r_g - h + r) - \pi r_g^2\right]E_a}{D}\frac{d\varepsilon_g}{dx} - \frac{\pi r_g^2 E_g}{D}\frac{d\varepsilon_g}{dx} \quad (r_g < r < r_a) \tag{11}$$

$$\tau(x,r) = -\frac{\left(D(H - r_g - h + r_a) - \pi r_g^2\right)E_a}{D}\left(\frac{r_m - r}{r_m - r_a}\right)\frac{d\varepsilon_g}{dx} - \frac{\pi r_g^2 E_g}{D}\left(\frac{r_m - r}{r_m - r_a}\right)\frac{d\varepsilon_g}{dx} \quad (r_a < r < r_m) \tag{12}$$

Because the length of the optical fiber is far more than the diameter, the radial displacement could be ignored, the following equation is obtained:

$$\tau(x,r) = G\gamma(x,r) = G\left(\frac{\partial u}{\partial r} + \frac{\partial v}{\partial r}\right) \cong G\frac{du}{dr} \tag{13}$$

Based on the shear lag theory, there is a relative displacement between the matrix, the adhesive layer and the optical fiber, then the relative displacements of each layer are determined by its shear strain.

$$u(x,r_a) - u(x,r_g) = \int_{r_g}^{r_a} \gamma(x,r)dr \tag{14}$$

$$u(x,r_m) - u(x,r_a) = \int_{r_a}^{r_m} \gamma(x,r)dr \tag{15}$$

Integrating Eq. (14) from ($r_g$, $r_a$) and Eq. (15) from ($r_a$, $r_m$), respectively, then take the derivative with respect to x, yields

$$\frac{du(x,r_a)}{dx} - \frac{du(x,r_g)}{dx} = \varepsilon(x,r_a) - \varepsilon(x,r_g) = \int_{r_g}^{r_a}\frac{d\gamma(x,r)}{dx}dr = \frac{1}{G_a}\int_{r_g}^{r_a}\frac{d\tau(x,r)}{dx}dr \tag{16}$$

$$\frac{du(x,r_m)}{dx}-\frac{du(x,r_a)}{dx}=\varepsilon(x,r_m)-\varepsilon(x,r_a)=\int_{r_a}^{r_m}\frac{d\gamma(x,r)}{dx}dr=\frac{1}{G_m}\int_{r_a}^{r_m}\frac{d\tau(x,r)}{dx}dr \tag{17}$$

Substitute Eq. (4), Eq. (8) and Eq. (9) into Eq. (16) and Eq. (17), respectively,

$$\varepsilon_a(x)-\varepsilon_g(x)=-\left[\frac{\left[D\left(H-h-\frac{r_g}{2}+\frac{r_a}{2}\right)-\pi r_g^2\right]E_a\left(r_a-r_g\right)}{G_aD}+\frac{\pi r_g^2E_g\left(r_a-r_g\right)}{G_aD}\right]\frac{d\varepsilon_g^2}{dx^2} \tag{18}$$

$$\varepsilon_m(x)-\varepsilon_a(x)=\left[\frac{\left[D(H-h-r_g+r_a)-\pi r_g^2\right]E_a(r_a-r_m)}{2G_mD}+\frac{\pi r_g^2E_g(r_a-r_m)}{2G_mD}\right]\frac{d\varepsilon_g^2}{dx^2} \tag{19}$$

By Eq. (18) and Eq. (19), yields

$$\varepsilon_m(x)-\varepsilon_g(x)=-\left\{\begin{array}{l}\dfrac{\left[D\left(H-h-\frac{r_g}{2}+\frac{r_a}{2}\right)-\pi r_g^2\right]E_a\left(r_a-r_g\right)}{G_aD}\\+\dfrac{\pi r_g^2E_g\left(r_a-r_g\right)}{G_aD}\\-\dfrac{\left[D(H-h-r_g+r_a)-\pi r_g^2\right]E_a(r_a-r_m)}{2G_mD}\\+\dfrac{\pi r_g^2E_g(r_a-r_m)}{2G_mD}\end{array}\right\}\frac{d\varepsilon_g^2}{dx^2}=-\frac{1}{k^2}\frac{d\varepsilon_g^2}{dx^2} \tag{20}$$

$$k^2=\left\{\begin{array}{l}\dfrac{\left\{\left[D\left(H-h-\frac{r_g}{2}+\frac{r_a}{2}\right)-\pi r_g^2\right]E_a+\pi r_g^2E_g\right\}\left(r_a-r_g\right)}{G_aD}\\-\dfrac{\left\{\left[D(H-h-r_g+r_a)-\pi r_g^2\right]E_a+\pi r_g^2E_g\right\}(r_a-r_m)}{2G_mD}\end{array}\right\}^{-1} \tag{21}$$

where k is strain lag parameter which contains the effects of the optical fiber, adhesive layer and matrix.

Differentiating Eq. (20) with respect to x yields

$$\frac{d^2\varepsilon_g}{dx^2}-k^2\varepsilon_g+k^2\varepsilon_m=0 \tag{22}$$

The general solution of Eq. (22) is the following form:

$$\varepsilon_g(x)=c_1e^{kx}+c_2e^{-kx}+\varepsilon_m \tag{23}$$

where c1 and c2 are determined by boundary conditions.

Since one end of the fiber has no constraints, the other end of the fiber near the grating is approximately the measured strain of FBG which is $\varepsilon_f$ , the boundary conditions can be expressed as:

$$\varepsilon_g(0)=0$$
$$\varepsilon_g(L)=\varepsilon_f \tag{24}$$

Substitute Eq. (24) into Eq. (23):

$$c1=\frac{\varepsilon_f+(e^{-kL}-1)\varepsilon_m}{2\sinh(kL)}$$
$$c2=-\frac{\varepsilon_f+(e^{kL}-1)\varepsilon_m}{2\sinh(kL)} \tag{25}$$

So the optical fiber strain equation in the bonding area is expressed as:

$$\varepsilon_g(x)=\frac{\varepsilon_f+(e^{-kL}-1)\varepsilon_m}{2\sinh(kL)}e^{kx}-\frac{\varepsilon_f+(e^{kL}-1)\varepsilon_m}{2\sinh(kL)}e^{-kx}+\varepsilon_m \tag{26}$$

According to Fig. 1, the measured strain of FBG and the strain of the matrix can be expressed as:

$$\varepsilon_f=\frac{\Delta L_f}{L_f} \tag{27}$$

$$\varepsilon_m=\frac{\Delta L_f+2\Delta L}{L_f+2L} \tag{28}$$

According to the synchronous deformation of optical fiber, adhesive layer and matrix, Eq. (29) can be obtained:

$$\Delta L=\int_0^L \varepsilon_g(x)dx$$
$$=\frac{\varepsilon_m(2k^2-2(k^2+1)\cosh(kL)+2kL\sinh(kL))}{2k\sinh(kL)}+\frac{\varepsilon_f(k^2e^{kL}-k^2+e^{-kL}-1)}{2k\sinh(kL)} \tag{29}$$

By Eq. (27), Eq. (28) and Eq. (29), the equation of the average strain transfer rate from the optical fiber to the matrix is following:

$$\frac{\varepsilon_f}{\varepsilon_m}=\frac{2(k^2+1)-kL_f\sinh(kL)-(2k^2+1)\cosh(kL)}{1-kL_f\sinh(kL)+k^2(e^{kL}-1)-e^{-kL}} \tag{30}$$

## 3 Parametric Analysis and Numerical Validation

### *3.1 Parametric Analysis*

The parametric analysis is performed using Eq. (30) to investigate the influences of parameters of the optical fiber, adhesive layer and matrix on the average strain transfer rate. Since Parameters of optical fiber are considered as known quantities (see Tab. 1) and are not taken into account. So, the effects of parameters on the average strain transfer rate is concentrated in the adhesive layer and the matrix. The physical parameters of the adhesive layer and the matrix are shown in Tab. 2 and Tab. 3.

**Table 1:** Mechanical properties of the optical fiber

| Material Parameter | Symbol | Value |
|---|---|---|
| Young's modulus (Pa) | $E_g$ | $7.2\times10^{10}$ |
| Radius (m) | $r_g$ | $62.5\times10^{-9}$ |

**Table 2:** Mechanical properties of the adhesive layer

| Material Parameter | Symbol | Value |
|---|---|---|
| Poisson's ratio | $\mu$ | 0.24~0.44 |
| Young's modulus (Pa) | $E_a$ | (0.05~4) $\times 10^9$ |
| Bonding length (m) | $L$ | (0.1~2) $\times 10^{-3}$ |
| Bonding width (m) | $D$ | (0.5~4) $\times 10^{-3}$ |
| Bonding height (m) | $H$ | (0~2.5) $\times 10^{-3}$ |
| Bottom thickness (m) | $h$ | (0.1-2) $\times 10^{-3}$ |

**Table 3:** Mechanical properties of the matrix

| Material Parameter | Symbol | Value |
|---|---|---|
| Shear modulus (Pa) | $G_m$ | (0.1~77) $\times 10^9$ |
| Matrix thickness affected by adhesive layer (m) | $r_m$- $r_a$ | (0.0~3) $\times 10^{-3}$ |

In the analysis, it is assumed that a single parameter in the average strain transfer rate changes while the other parameters remain unchanged. The initial values of parameters of the adhesive layer and matrix are set as follows: $E_a = 4 \times 10^9$ Pa, $\mu = 0.34$, $H = 0.2425 \times 10^{-3}$ m, $h = 0.1 \times 10^{-3}$ m, $D = 4 \times 10^{-3}$ m, $L = 2 \times 10^{-3}$ m, $L_f = 20 \times 10^{-3}$ m, $G_m = 77 \times 10^9$ Pa, $r_m$- $r_a = 0.3 \times 10^{-3}$ m.

It is concluded that the average strain transfer rate of Refs. [21] and in this paper is obtained using Eq. (30) is 94.37% and 99.95%, respectively. The model proposed in this paper takes into account the multiple factors of the adhesive layer and the matrix, therefore, which has a high average strain transfer rate. In addition, Refs. [22] deduces the strain transfer equation based on the symmetric structure, which is different from the asymmetric structure of Refs. [21] and Eq. (30) of this paper.

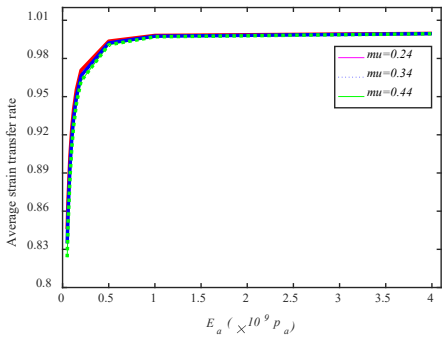


(a)

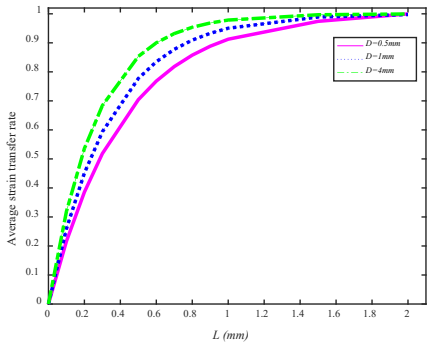


(b)

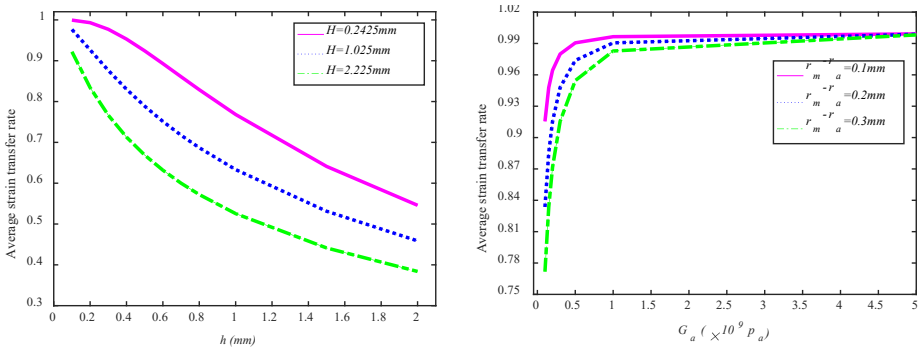


(c) (d)

**Figure 5:** Influence of the parameters of adhesive layer and matrix on average strain transfer rate (a) Effect of Young's modulus and Poisson's ratio of the adhesive layer; (b) Effect of bonding width and length of adhesive layer; (c) Effect of the bonding height and bottom thickness of the adhesive layer; (d) Effect of shearing modulus of matrix and thickness affected by adhesive layer

Fig. 5 shows the influence of the parameters of the adhesive layer and the matrix on average strain transfer rate both grating ends surface-bonded FBG. Fig. 5(a) shows that the average strain transfer rate increases with increasing the Young's modulus of the adhesive layer, but decreases with increasing the Poisson's ratio. Fig. 5(b) shows that the average strain transfer rate increase with increasing both the bonding width and the single bonding length of the adhesive layer, respectively. Fig. 5(c) show that the average strain transfer rate decreases with increasing both the bonding height and the bottom thickness of the adhesive layer, respectively. In Fig. 5(d), the average strain transfer rate increases with the increase of shearing modulus of the matrix. When the shear modulus of the matrix is small ($< 1 \times 10^9$ Pa), the matrix thickness affected by the adhesive layer has a significant influence on the average strain transfer rate.

Base on the above analysis, it is possible to obtain an average strain transfer rate of exceeding 95% in the range of Tab. 2 and Tab. 3 for the grating ends surface-bonded FBG when the parameters are satisfied as following: $L > 1.5 \times 10^{-3}$ m, $D > 1.5 \times 10^{-3}$ m, $h < 0.2 \times 10^{-3}$ m, $H < 0.4 \times 10^{-3}$ m. It can be concluded that the bonding width, single length, height and bottom thickness of the adhesive layer with grating ends surface-bonded FBG are all greatly reduced compared with the grating surface-bonded FBG, which simplifies the process of packaging sensor and meets the accuracy of FBG used in scientific research and engineering application.

### *3.2 Numerical Validation*

In order to validate the theoretical prediction Eq. (30), a numerical study by finite element method (FEM) using commercial software ANSYS Workbench 17.0 is conducted. The parameters of the adhesive layer are set as follows: $E_a = 4 \times 10^9$Pa, $\mu = 0.34$, $H = 0.2425 \times 10^{-3}$ m, $h = 0.1 \times 10^{-3}$ m, $D = 4 \times 10^{-3}$ m, and $L = (0.1\sim2) \times 10^{-3}$ m. Where the single bonding length, width and height of the matrix are $30 \times 10^{-3}$ m, $20 \times 10^{-3}$ m and $1 \times 10^{-3}$ m, respectively.

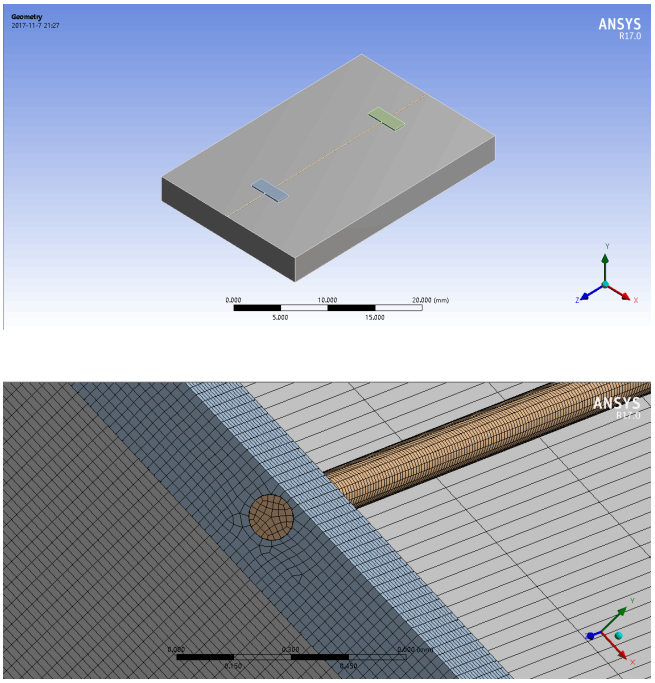


**Figure 6:** Finite element meshes

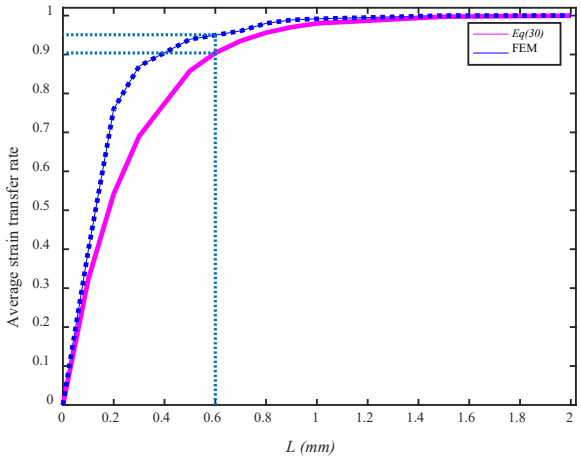


**Figure 7:** Comparison of the average strain transfer rate with the bonding length by FEM and Eq. (30)

Fig. 6 shows that the schematic diagram of both grating ends surface-bonded FBG and the finite element meshes. Fig. 7 shows the comparison of the average strain transfer rate with the single bonding length by FEM and Eq. (30), it can be seen that the theoretical predictions are in agreement with FEM results in the trends, and the theoretical prediction is slightly less than the numerical solution. When the single bonding length is over $0.6 \times 10^{-3}$ m, the error between Eq. (30) and FEM is less than 5%.

The main reasons for the error are as follows:

(1) In this paper, the corresponding assumptions and simplifications are made when the theoretical model is established, so the theoretical predictions are different from FEM.

(2) With the increase of bonding length, the average strain transfer rate of both results is increasing. In numerical calculation, there is a stress singularity at the end of the adhesive layer when the bonding

length is smaller, which makes the average strain transfer rate is larger, so that the theoretical solution and numerical solution has bigger error.

## 4. Experimental Test Results

### *4.1. Experimental Method*

The experiment tests were performed to verify the theoretical predictions. One end of the FBG with removing the coating is adhered to the surface of the equal-intensity cantilever beam, and the other end is bonded by the same way after applying the prestressing. The temperature compensation is made by another bare FBG. Fig. 8 show the schematic and the physical map both the grating ends bonded-surface FBG and resistance strain gage are bonded on the equal-intensity cantilever beam.

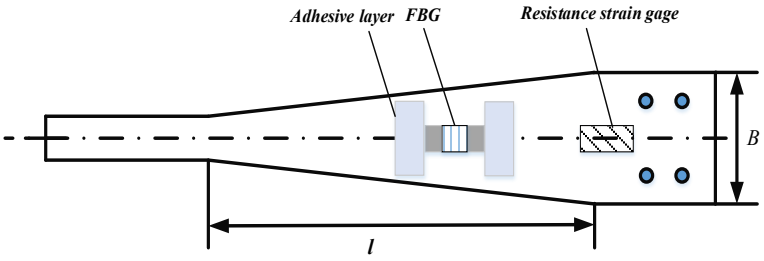


(a)

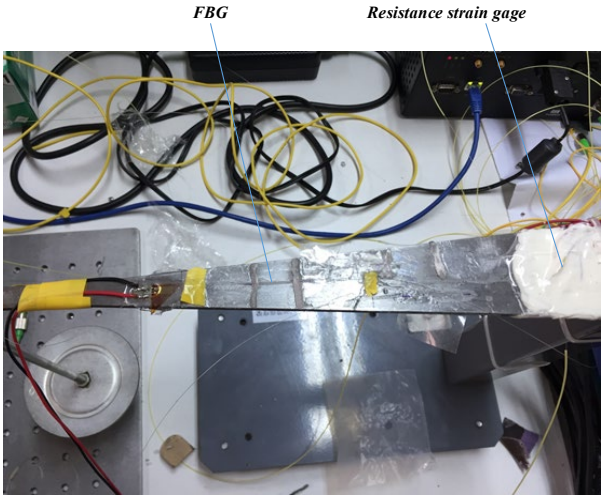


(b)

**Figure 8:** Grating ends bonded-surface FBG and strain gage in the equal-intensity cantilever beam. (a) the schematic; (b) the physical map

The equal-intensity cantilever beam is made of stainless steel in the experiment. Its size is $l \times B \times h = 300 \times 10^{-3}$ m $\times$ $45.9 \times 10^{-3}$ m $\times$ $3.5 \times 10^{-3}$ m.

where $l$ is the distance between the load fulcrum and the cantilever beam supporting, $B$ is the width at the supporting, and $h$ is the thickness of the cantilever beam.

The surface strain of the cantilever beam is as follows:

$$\varepsilon = \frac{\sigma}{E} = \frac{1}{E} \times \frac{M}{W} = \frac{6}{E} \times \frac{P}{h^2} \times \frac{l}{B} \tag{31}$$

where $\sigma$ is the tensile stress, $M$ is the bending moment at the supporting of the cantilever beam, $P$ is the load; $W$ is the shear strength, $E = 210 \times 10^9$ Pa. The surface strain of the cantilever beam is calculated from Eq. (31) is $149.393 \times 10^{-6}$ per kilogram.

MOI-130 demodulator was used for data acquisition in the experiment. The center wavelength of FBG is 1532.308 nm, the bonding parameters of the adhesive layer are as follows: $D = 20 \times 10^{-3}$ m, $L = 3 \times 10^{-3}$ m, $H = 2 \times 10^{-3}$ m, $h = 0.1 \times 10^{-3}$ m, the average strain transfer rate is 0.9841 using Eq. (30).

### *4.2 Experiment Results*

Fig. 9 shows the data which is acquired from the FBG and the resistance strain gage after every loading force is 10 *kN*, 10 *kN,* 10 *kN*, 5 *kN* and 5 *kN*, respectively. It is shown that FBG are in great agreement with strain gage, which proves the validity of the acquired data. It takes the average strain value after each loading in Fig. 9 as the strain under this loading.

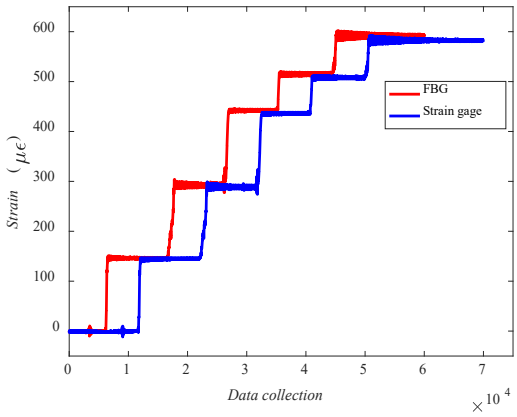


**Figure 9:** Strain is acquired FBG and strain gage

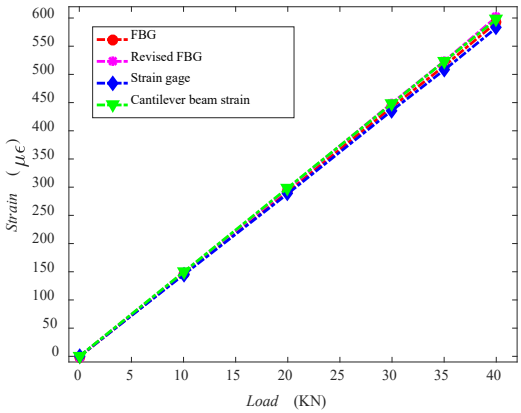


**Figure 10:** Strain measurement comparison

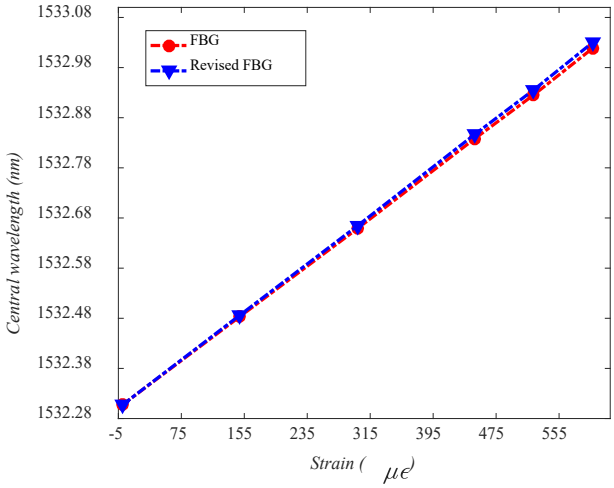


**Figure 11:** Relation between the central wavelength of FBG and the theoretical strain

Fig. 10 show the comparison among the original strain of FBG, revised strain of FBG (that is, taking into account average strain transfer), the strain of the resistance strain gage and the theoretical strain of equal-intensity cantilever beam. In Fig. 10, the linearity of the original strain measured by FBG is 0.99996, the fitting equation is $y = 14.7963x - 1.7948$, and stress sensitivity is 14.7963 $\mu\varepsilon$ / *kN* ; the linearity of the revised strain measured by FBG is 0.99996, the fitting equation is $y = 15.0354x - 1.8238$, and the stress sensitivity is 15.0354 $\mu\varepsilon$ / *kN* ; the linearity of the strain measured by the resistance strain gage is 0.99998, the fitting equation is $y = 14.5605x - 1.1058$, and stress sensitivity is 14. 5605 $\mu\varepsilon$ / *kN* ; the fitting equation for the theoretical strain of the equal-intensity cantilever beam is $y = 14.9393x + 2.5169 \times 10^{-13}$, and the

stress sensitivity is 14.9393 $\mu\varepsilon / kN$. It can be seen that the stress sensitivity after considering average strain transfer rate is closer to the theoretical stress sensitivity of the equal-intensity cantilever beam.

Fig. 11 shows that the correspondence between the wavelength of the grating ends surface-bonded FBG considering average strain transfer rate and the theoretical strain of the cantilever beam, the linearity of original FBG is 0.99996, the fitting equation is $y = 0.0011885x + 1532.3058$, and the strain sensitivity is 1.1885 $pm / \mu\varepsilon$. The linearity of revised FBG is 0.99996, the fitting equation is $y = 0.0012077\ x + 1532.3058$, and the strain sensitivity is 1.2077 $pm / \mu\varepsilon$.

The relation between wavelength relative drift and unit strain is considered only when the center wavelength of FBG caused by axial strain [23-25]:

$$\frac{\Delta\lambda_B}{\lambda_B} = \left\{1 - \frac{n^2_{eff}}{2}\left[p_{12} - (p_{11} + p_{12})v\right]\right\} \cdot \varepsilon = K_\varepsilon \cdot \varepsilon \tag{32}$$

where $\Delta\lambda_B$ is the wavelength shift, $\lambda_B$ is the center wavelength. For germanium-doped silica fiber, $p_{11} = 0.121$, $p_{12} = 0.270$, $v = 0.17$, $n_{eff} = 1.456$, then $K_\varepsilon \approx 0.784$, when $\lambda_B =$ 1532.308 nm, the wavelength shift per microstrain using Eq. (32) is 1.201 pm.

From the above, it can be concluded that the strain coefficient error is 1.04% when average strain transfer is not considered, and the strain coefficient error is 0.56% when average strain transfer is considered. Therefore, the strain of the revised FBG is closer to the theoretical value.

## 5 Conclusions

The grating ends bonding FBG sensor has been widely used for health monitoring of large structures. Based on the shear lag theory, this paper studied the strain transfer mechanism of the grating ends surface-bonded FBG and builds up the average strain transfer model from the matrix to the optical fiber. A selection scheme of bonding parameters of the grating ends surface-bonded FBG is given by the proposed model. Compared with the existing methods, the measurement accuracy is improved, and the packaging process is simplified. The experiment tests were performed to verify the theoretical predictions by which the resistance strain gage and FBG are fixed on the equal-intensity cantilever beam, it shows that the two methods have good consistency. The proposed model provides a theoretical basis for the design and application of the grating ends surface-bonded FBG strain sensor.

**Acknowledgments:** This project was supported State Administration for Market Regulation Research Program(S2019MK315) and CSEI Research Program(2019-Youth-08).

## References

1. Cheng, C., Lo, Y., Li, W. (2010). Accurate simulations of reflective wavelength spectrum of surface-bonded fiber Bragg grating. *Applied Optics, 49,* 3394-3402.
2. Nanni, A., Yang, C. C., Pan, K., Wang, J. S., Jr, R. R. M. (1991). Fiber-optic sensor for concrete strain/stress measurement. *ACI Materials Journal, 88(3),* 257-264.
3. Pak, Y. E. (1992). Longitudinal shear transfer in fiber optic sensors. *Smart Materials and Structures, 1(1),* 57-62.
4. Ansari, F., Yuan, L. (1998). Mechanics of bond and interface shear transfer in optical fiber sensors. *Journal of Engineering Mechanics, 128(4),* 385-394.
5. Lau, K., Yuan, L., Zhou, L. (2001). Strain monitoring in FRP laminates and concrete beams using FBG sensors. *Composite Structures, 251,* 9-20.
6. Ren, L., Song, G. (2006). Strain transferring analysis of fiber Bragg grating sensors. *Optical Engineering, 45(2),* 409-411.
7. Li, Q., Li, G., Wang, G., Ansari, F., Liu, Q. (2002). Elastoplastic bonding of embedded optical fiber sensors in concrete. *Journal of Engineering Mechanics, 128,* 471-478.

8. Zhou, J., Zhou, Z., Zhang, D. (2010). Study on strain transfer characteristics of fiber Bragg grating sensors. *Journal of Intelligent Material Systems and Structures, 21,* 1117-1122.
9. Wang, H. P., Zhou, Z. (2014). Advances of strain transfer analysis of optical fiber sensors. *Pacific Science Review, 16(1),* 8-18
10. Li, H. N., Zhou, G. D., Ren, L. (2009). Strain transfer coefficient analyses for embedded fiber Bragg grating sensors in different host materials. *Journal of Engineering Mechanics, 135(12),* 1343-1353.
11. Ling, H. Y., Lau, K. T., Cheng, L., Chow, K. W. (2005). Embedded fiber Bragg grating sensors for non-uniform strain sensing in composite structures. *Measurement Science and Technology, 16,* 2415-2424.
12. Li, Q. B., Li, G., Yuan, L. B. (2004). Calibration of embedded fiber optic sensor in concrete under biaxial compression. *Measurement, 35(3),* 303-310.
13. Wu, R. J., Zheng, B. L., Fu, K. K. (2014). Study on strain transfer of embedded fiber Bragg grating sensors. *Optical Engineering, 53(8),* 085105-085105.
14. Wan, K. T., Leung, C. K. Y., Olson, N. G. (2008). Investigation of the strain transfer for surface-attached optical fiber strain sensors. *Smart Materials & Structures, 17(3),* 035037.
15. Wan, K. T. (2014). Quantitative sensitivity analysis of surface attached optical fiber strain sensors. *Sensors Journal IEEE, 14(6),* 1805-1812.
16. Her, S. C., Huang, C. Y. (2011). Effect of Coating on the strain transfer of optical fiber sensors. *Sensors, 11(7),* 6926-6941.
17. Wang, Q. B., Qiu, Y., Zhao, H. T., Chen, J. (2012). Analysis of strain transfer of six-layer surface-bonded fiber Bragg gratings. *Applied Optics, 51(18),* 4129-4138.
18. Zhao, H. T., Wang, Q. B., Qiu, Y. (2012). Strain transfer of surface-bonded fiber Bragg grating sensors for airship envelope structural health monitoring. *Journal of Zhejiang University Science A: Applied Physics & Engineering, 13(7),* 568-545.
19. Tian, S. Z., Zhang, G. Q., Wang, D. P. (2014). Study on strain transfer mechanism of surface fiber bragg grating sensor. *Chinese Journal of Lasers, 41(8),* 0805005-1-0805005-6.
20. Li, W. Y., Cheng, C. C., Lo, Y. L. (2009). Investigation of strain transmission of surface-bonded FBGs used as strain sensors. *Sensors and Actuators A: Physical, 149,* 201-207.
21. Wu, J., Chen, W. M., Yu, K. (2016). Strain sensing properties of grating ends packaged FBG sensors. *Acta Photonica Sinica, 45(2),* 79-83.
22. Sun, L., Li, C., Li, J., Zhang, C., Ding, X. (2017). Strain transfer analysis of a clamped fiber bragg grating sensor. *Applied Sciences, 7,* 188.
23. Shih, M. C., Ko, C. L., Yang, C. Y. (2008). Dynamic strain monitoring by wavelength locking between two fiber Bragg gratings fiber sensing system. *Optics and Lasers in Engineering, 46(7),* 546-549.
24. Wagreich, R. B., Altia, W. A., Singh, H., Sirkis, J. S. (1996). Effects of diametric load on fibre Bragg gratings in low birefringence fibre. *Electronics Letters, 32(13),* 1223-1224.
25. Gafsi, R., Sherif, M. A. E. (2000). Analysis of induced-birefringence effects on fiber Bragg gratings. *Optical Fiber Technology, 6(3),* 299-323.